AGU PUBLICATIONS

JGR

Journal of Geophysical Research: Space Physics

RESEARCH ARTICLE
10.1002/2016JA023830

Transpolar arcs observed simultaneously in both hemispheres

J. A. Carter[1], S. E. Milan[1,2], R. C. Fear[3], M.-T. Walach[1,4], Z. A. Harrison[1], L. J. Paxton[5], and B. Hubert[6]

[1]Department of Physics and Astronomy, University of Leicester, Leicester, UK, [2]Birkeland Centre for Space Science, Department of Physics and Technology, University of Bergen, Bergen, Norway, [3]Physics and Astronomy, University of Southampton, Southampton, UK, [4]Department of Physics, University of Lancaster, Lancaster, UK, [5]Applied Physics Laboratory, The Johns Hopkins University, Laurel, Maryland, USA, [6]Laboratory of Planetary and Atmospheric Physics, University of Liège, Liège, Belgium

Key Points:
- Two transpolar arcs are observed simultaneously in both hemispheres with unprecedented instrumental coverage
- The positions of the arcs at formation mirror about the midnight meridian in each hemisphere and suggest a complex magnetic topology
- Subsequent motion of the arcs is consistent with the direction of the B_y-dominated interplanetary magnetic field

Correspondence to:
J. A. Carter,
jac48@leicester.ac.uk

Citation:
Carter, J. A., S. E. Milan, R. C. Fear, M.-T. Walach, Z. A. Harrison, L. J. Paxton, and B. Hubert (2017), Transpolar arcs observed simultaneously in both hemispheres, *J. Geophys. Res. Space Physics*, *122*, 6107–6120, doi:10.1002/2016JA023830.

Received 12 JAN 2017
Accepted 16 MAY 2017
Accepted article online 19 MAY 2017
Published online 13 JUN 2017

Abstract Two coexisting transpolar arcs are observed on 31 August 2005. We track the formation and motion of the arcs in both the Northern and Southern Hemispheres, using data from two independent satellites (Imager for Magnetopause to Aurora Global Exploration and a Defence Meteorological Satellite Program satellite). The observations are supported by supplementary ground-based ionospheric convection data from the Super Dual Auroral Radar Network. The two arcs form during a period of northward interplanetary magnetic field. Following a change in the direction of the interplanetary magnetic field B_Y component from negative to positive, the dawnside arc traverses the polar cap to the duskside in the Northern Hemisphere. Over the same time period and in the Southern Hemisphere, the duskside arc traverses the polar cap to the dawnside. A complex magnetic field line topology resulting in the coexistence of two tongues of closed field lines protruding into the otherwise open polar cap is implied. We discuss these observations in terms of magnetic conjugacy and a model of transpolar arcs formation.

Plain Language Summary Aurora emissions are normally found in a large ring, the "auroral ovals" that encircle the globe at high magnetic latitudes around the northern and southern poles. The "polar cap" areas poleward of these rings are often devoid of auroras. "Transpolar arcs," however, are large-scale spurs of emission that extend from the auroral oval into the dark polar cap. There is still controversy about how a transpolar arc can form in the polar cap region. We simultaneously observe two transpolar arcs in each polar cap, using two independent satellites. In addition, the arcs form at opposite sides of the polar cap in each hemisphere. One of the arcs is then seen to move across the polar cap, in opposite directions in each hemisphere. The formation and movement of the arcs is consistent with a model of transpolar arc formation, whereby arcs will form at mirror positions about the midnight line in each hemisphere. However, the arrangement of the magnetic field implied by seeing two simultaneous arcs must be complex.

1. Introduction

Large-scale polar cap arcs, primarily observed via spacecraft-based auroral imaging, are a class of auroral features that protrude from the nightside auroral oval into the otherwise dark polar cap region. These polar cap arcs, also known as Sun-aligned arcs or theta aurora, may extend from the nightside all the way to the dayside of the polar cap [*Frank et al.*, 1982]. Transpolar arcs (TPAs) occur primarily under northward interplanetary magnetic field (IMF) [*Berkey et al.*, 1976; *Gussenhoven*, 1982]. Other large-scale polar cap arc phenomena, such as bending arcs, may occur under southward IMF [*Carter et al.*, 2015]. The location in magnetic local time (MLT) where a TPA forms has been shown to be dependent on the IMF B_Y orientation several hours prior to the appearance of the arc [*Fear and Milan*, 2012a]. *Gusev and Troshichev* [1986] noted that for the Northern and Southern Hemispheres, TPAs form on opposite sides of the polar cap for the same sense of IMF B_Y. Subsequent motion of the arc duskward or dawnward has been associated with a change in the IMF B_Y component [*Kullen et al.*, 2002; *Fear and Milan*, 2012a].

Competing models of the formation of TPAs have been comprehensively reviewed by *Fear and Milan*, 2012a [2012a, and references therein]. These models encompass a range of explanations regarding formation of the arcs, with some models suggesting that arcs form on open polar cap field lines and some models advocating

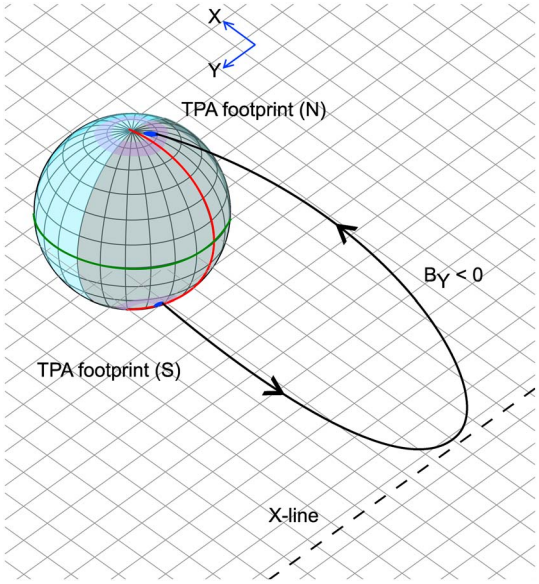

Figure 1. Schematic of one of the magnetic field lines (black line) footprints a TPA (dark blue regions) at formation on the nightside of the Earth (shaded region of the gridded sphere). The footprints are mirrored about the midnight meridian (red line) in each hemisphere. Purple regions indicate the approximate positions of the auroral oval.

formation on closed field lines. *Reidy et al.* [2017] have recently provided observational evidence that polar cap arcs on closed field lines may occur simultaneously with other polar cap auroras on open field lines. However, this controversy has yet to be categorically resolved.

In one such model [*Milan et al.*, 2005], the TPA forms as a tongue of closed magnetic flux, embedded in the otherwise open-flux polar cap region. This can occur following magnetic reconnection in the tail, under northward IMF conditions with a significant B_Y component such that the tail is twisted [e.g., *Grocott et al.*, 2003, 2004]. The TPA will form at an MLT offset from the midnight meridian, dependent on the sign and magnitude of the B_Y component sometime prior to the arc's appearance. The MLT position of the TPA in the Northern Hemisphere will be mirrored about the midnight meridian in the Southern Hemisphere (see Figure 1). During the period of tail reconnection, sequential field lines are closed in the tail, so that the TPA gradually extends toward higher latitudes. Strong azimuthal ionospheric flows along the nightside auroral oval are associated with reconnection in a twisted tail and hence are often observed when TPAs are present [*Milan et al.*, 2005; *Fear and Milan*, 2012b]. Once formed, the arc may move, as a result of "lobe" reconnection occurring at the high-latitude magnetopause. This lobe stirring causes a redistribution of open magnetic flux in the polar cap. The contemporaneous sign and magnitude of IMF B_Y component, which controls the sense of magnetic tension forces, will therefore control the motion of the TPA. Each hemisphere experiences distinct lobe reconnection, and therefore, the motion of a TPA observed in the Northern Hemisphere may be independent from that in the south. *Goudarzi et al.* [2008] also presented a case in which a TPA moved across the polar cap in response to a southward turning of the IMF and the addition of new open flux to the polar cap by low-latitude reconnection. During this event the IMF had a significant B_Y component, so that in the Northern Hemisphere the new open flux was added to the dawnside polar cap, and the TPA correspondingly moved toward dusk. In both of these scenarios [*Milan et al.*, 2005 and *Goudarzi et al.*, 2008], the TPA moves as a consequence of the redistribution of open magnetic flux in the polar cap, embedded within which is the closed flux of the TPA, by magnetopause reconnection. Observations of TPAs (from a single hemisphere) using the IMAGE-SI13 filter [*Hubert et al.*, 2004] showed significant proton precipitation at the location of the arcs, suggesting that TPAs are threaded by closed field lines.

In this study we present observations of the simultaneous formation and motion of two TPAs in both hemispheres. In the past there have been few simultaneous observations of the Northern and Southern Hemisphere auroras via high-altitude imagers, which offer the possibility of observing a TPA in both hemispheres. *Obara et al.* [1988] used the EXOS-C satellite to measure ion and electron spectra associated with a TPA in the Southern Hemisphere, along with images from the Viking spacecraft of a TPA in the Northern Hemisphere. The authors concluded that they had observed the same conjugate structure in both hemispheres, at approximately the same local time. The TPAs were static over the course of their observations. *Huang et al.* [1989] used the auroral imager of the Dynamics Explorer 1 to observe a TPA in the Northern Hemisphere. Particle detectors on board the ISEE 1 spacecraft at the time detected increased particle fluxes in the Southern Hemisphere that the authors attributed to plasma sheet associated with the conjugate field line of the northern TPA. *Craven et al.* [1991] also used Dynamics Explorer 1, along with Viking to examine a TPA observed in both hemispheres. Although the arc appeared in each hemisphere on either side of the midnight meridian, the subsequent motion of the arcs in each hemisphere was independent. A recent set of U.S. Air Force Defense Meteorological Satellite Program (DMSP) particle precipitation data examined by *Watanabe and Hairston* [2016] was used

to identify a set of TPAs in both hemispheres. The authors concluded from the particle precipitation data only that example arcs moved in the opposite sense in each hemisphere and that motion reversed following a change in direction of the IMF B_Y component. *Østgaard et al.* [2003] presented two case studies in which they observed a TPA in one hemisphere but not in the other. They used data from both the Polar VIS Earth camera (sensitive at 130.4 nm) and the Imager for Magnetopause-to-Aurora Global Exploration (IMAGE) [*Mende et al.*, 2000a, 2000b] Far Ultraviolet instrument (using the SI13 filter, sensitive at 135.6 nm). *Østgaard et al.* [2003] also used DMSP data to observe spectra of the precipitating particles in the region of the TPAs. In the first case study presented, a TPA was seen only in the Northern Hemisphere, and in the second case study, a TPA was only seen in the Southern Hemisphere. In both cases, the authors presented evidence of ion precipitation, observed by DMSP, in the hemisphere of the TPA, which was consistent with the TPA being on closed field lines. However, they noted the lack of any such signature in the opposite hemisphere. The authors suggested that interhemispheric differences in conductivity, or the role that the IMF B_X component takes in determining where lobe reconnection is most likely, may play a role in the supression or lack of a TPA in the conjugate hemisphere. Although the authors noted that the ion signature was consistent with closed field lines, the lack of a TPA in the other hemisphere and the invocation of lobe reconnection are consistent with the TPA being on open field lines. The result of *Østgaard et al.* [2003] apparently contradicts what would be expected to be observed via the *Milan et al.* [2005] TPA formation mechanism and any other mechanism based on closed field lines, whereby a TPA would be observed in both, rather than just one hemisphere. The apparent contradicitons between observations to date demonstrate the need for interhemispheric observations of TPAs, which have previously been rare.

In this paper we use two independent imaging spacecraft to observe a pair of TPAs during a period exhibiting primarily northward IMF with a large B_Y component. We utilize high-altitude global images obtained by the IMAGE far ultraviolet instrument, along with low-latitude images of swaths of auroral emissions from the Special Sensor Ultraviolet Spectrographic Imagers (SSUSI) [*Paxton et al.*, 2002], which have flown on spacecraft of the DMSP program since 2005. This has provided near-simultaneous coverage of both hemispheres over part of the polar cap regions. We also employ data from the Super Dual Auroral Radar Network (SuperDARN) [*Chisham et al.*, 2007] to provide information regarding ionospheric convection flows. This set of data provides unprecedented coverage (in terms of time span and range of data sets used), to undertake a detailed study of the formation and evolution of a pair of simultaneously observed TPAs.

The paper is laid out as follows. In section 2 we describe the data sets that we use in our case study, and we present a detailed description of our case. In section 3 we discuss the TPAs observed in context of the *Milan et al.* [2005] model, and we conclude in section 4.

2. Observations

We present a case study from 31 August 2005. On this day, the IMAGE spacecraft took observations of the Southern Hemisphere auroras, whereas the DMSP (F16 satellite) provided observations of the auroras in swaths of both the Northern and Southern Hemispheres. Two TPAs were observed in each hemisphere.

We extract contemporaneous solar wind and auroral index data from the time-shifted OMNI data set [*King and Papitashvili*, 2005]. SuperDARN data from ground-based radars provide measurements of the ionospheric convection, and we use these data when available, to understand the magnetospheric dynamics that give rise to the formation and motion of the arcs. SuperDARN radars exist in both Northern and Southern Hemispheres, though we show observations from the Northern Hemisphere as much more comprehensive coverage is available.

Solar wind conditions for 07 to 13 UT on this date, geomagnetic auroral indices, and keograms from the sequence of IMAGE Wideband Imaging Camera (WIC) are shown in Figure 2. The solar wind density (Figure 2a) is high during this period, varying between 10 and 40 cm^{-3}. The solar wind speed (Figure 2b) is close to 400 km s^{-1} throughout; however, in combination with the increasing density, the external momentum flux impinging on the magnetosphere increases throughout the period. The IMF B_Y (Figure 2c) and B_Z (Figure 2d) components are expressed in geocentric solar magnetic coordinates (GSM). The IMF B_Y component (Figure 2c) changes from negative to positive just before 09:00 UT (along with a very short positive excursion at around 08:30 UT) and remains near +15 nT throughout the remainder of the period. The IMF is directed northward ($B_Z > 0$) for the majority of the interval, turning southward at 12 UT. We divide the total interval of time shown into four: (I) between 07:00 UT and 09:15 UT when the IMF is predominantly northward with a small negative

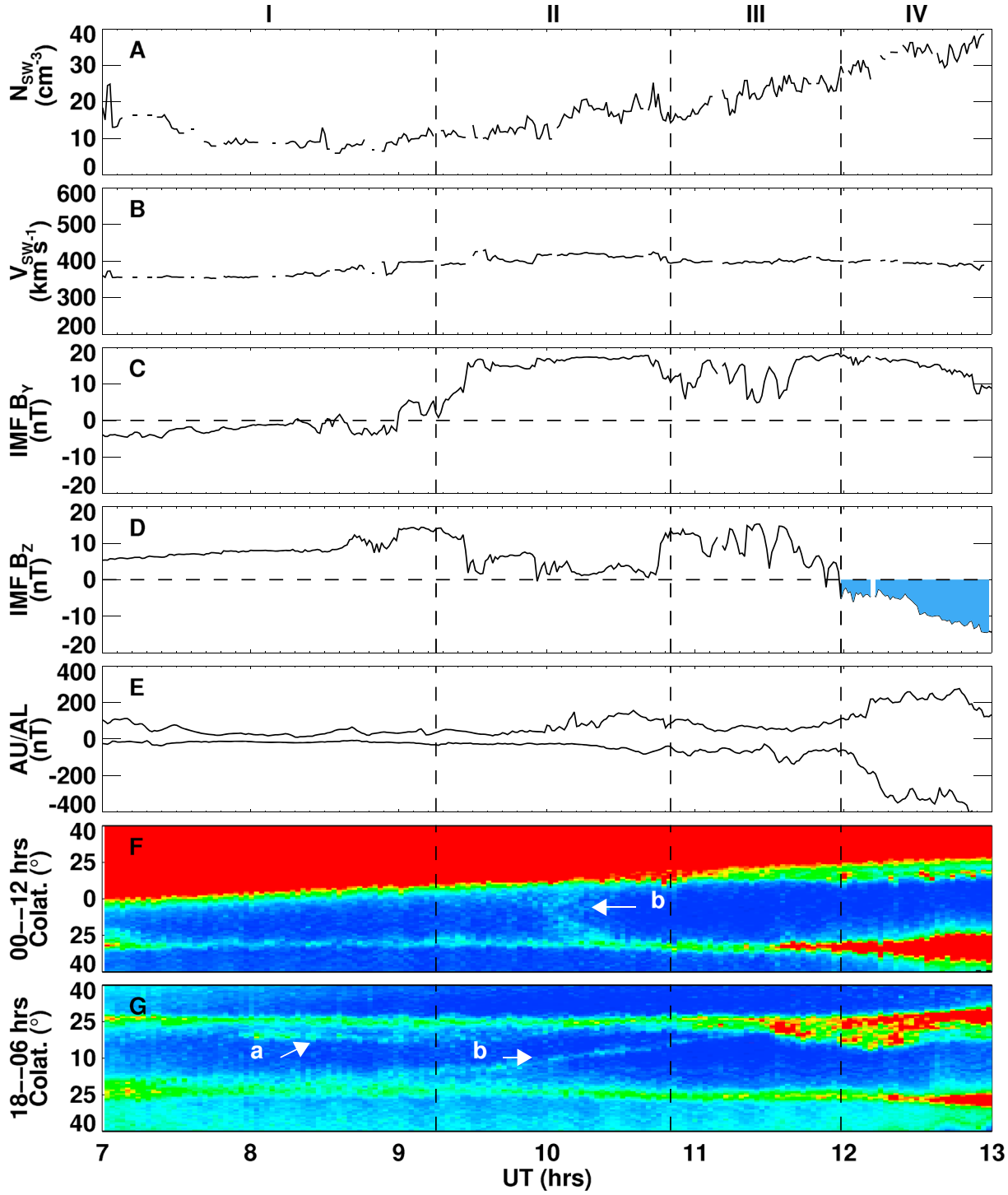

Figure 2. Solar wind and IMF conditions, auroral indices, and keograms for the case study period on 31 August 2005. The (a) solar density, (b) speed, (c) IMF B_Y, (d) IMF B_Z (southward IMF is highlighted in blue in Figure 2d) and (e) upper and lower auroral indices. Keograms from the IMAGE/WIC sequence across the (f) noon-midnight and (g) dusk-dawn meridians. Arcs are labeled in Figures 2f and 2g.

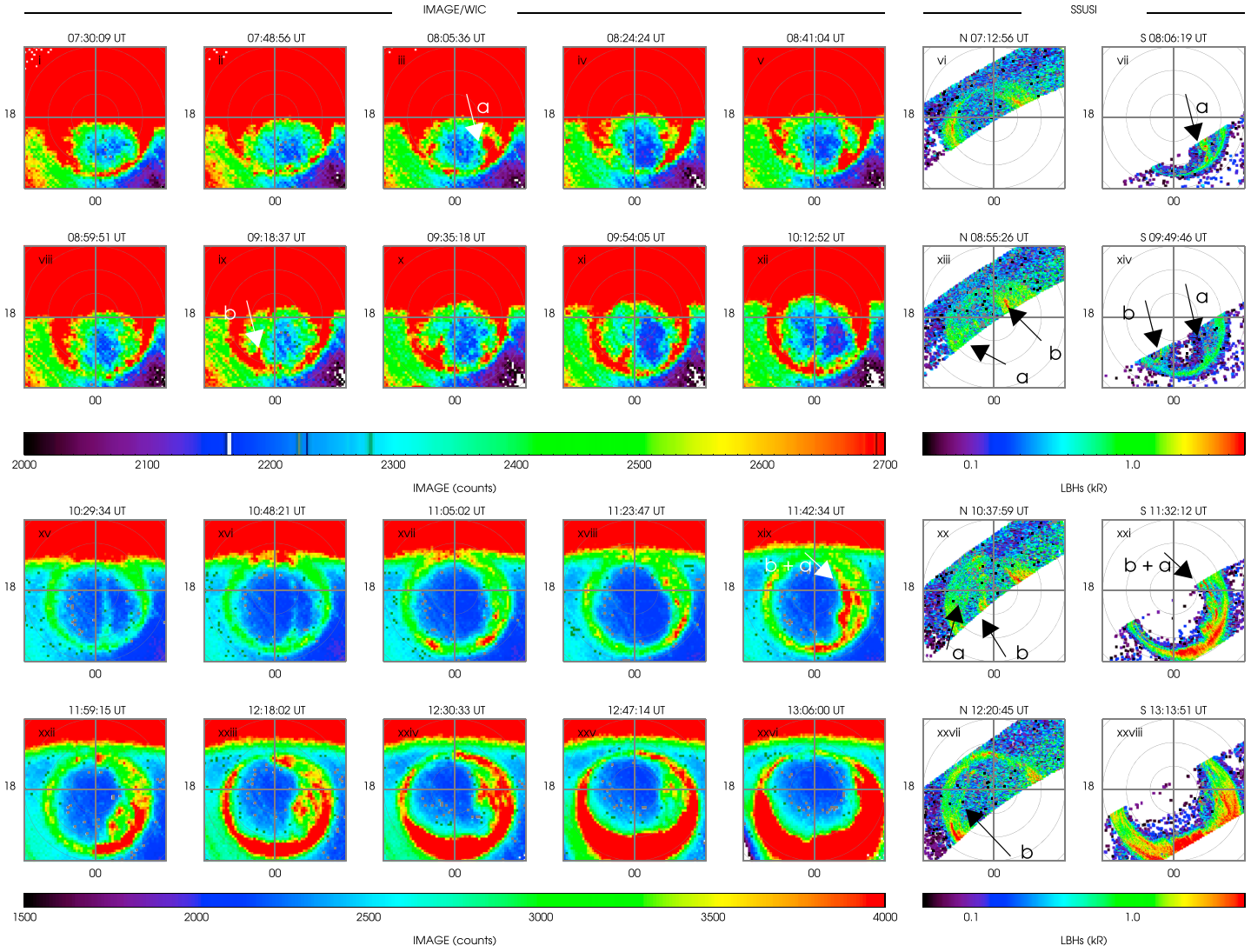

Figure 3. Sequence of select images from 31 August 2005 showing the evolution of the arcs. In the first five columns of each row we plot data taken from IMAGE/WIC of the Southern Hemisphere polar cap. In the last two columns of each row we show images from SSUSI (LBHs band) during high (absolute)-latitude polar passes of the DMSP F16 spacecraft from both hemispheres. Lines of geomagnetic latitude are plotted at intervals of 10°. The Sun is toward the top of each panel. Note the change of color scale in the figure.

B_Y component, (II) between 09:15 UT and 10:50 UT when the IMF is dominated by positive B_Y but with a small northward component, (III) when both B_Y and B_Z have similar positive magnitudes, and (IV) when the southward turning of the IMF occurs. In Figures 2f and 2g we plot keograms of the auroral emissions along the noon-midnight and dusk-dawn meridians, respectively, extracted from the IMAGE/WIC observations. The two observed arcs are labeled in Figure 2g. In Figure 2f dayglow is apparent in the noon sector, with the nightside oval at a colatitude of ~25° at the beginning of period I. The dusk-dawn meridian has been extracted from a row of pixels at 10° antisunward of the 18–06 h MLT line, to avoid the dayglow. In Figure 2g, at the beginning of period I, the dawn and dusk sector ovals are located at colatitudes of ~25°. During period I and as shown in Figure 2g, there is a gradual and slight decrease in polar cap area (the area between the two auroral bands) as the auroras move poleward. This is followed by a gradual increase in area, shown by the equatorward motion of the auroras to larger colatitudes, in periods II and the first part of period III. The buildup to a large geomagnetic substorm is noted in both keograms, which is seen in the contraction of the overall polar cap region toward the end of period III and in the brightening of the main auroral oval. There is a southward turning at 11:59 UT after which (period IV) the substorm commences. The commencement of the substorm is also reflected in the auroral indices (Figure 2e) and the intense brightenings in the keograms

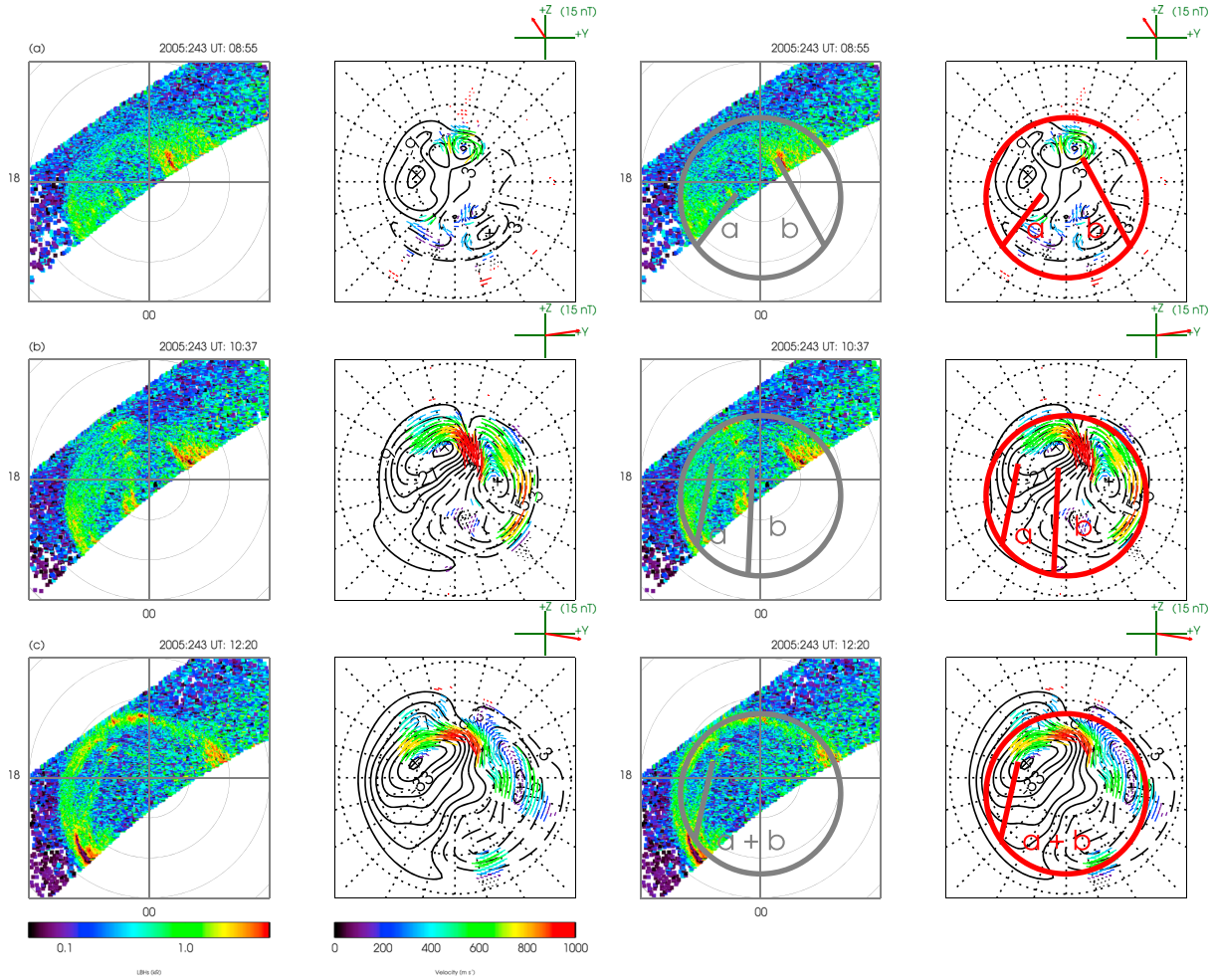

Figure 4. Select IMAGE/WIC images and SuperDARN ionospheric flows and electrostatic equipotential patterns for the Northern Hemisphere. Noon/dawn is toward the top/right. Panels in the right side columns include overlay positions of the TPAs. The IMF vector at the time of each row is given in the dial in the upper right of the SuperDARN panels.

(Figures 2f and 2g). In Figure 2g the first transpolar arc "a" is observed as a band of emission adjacent to the dawn sector oval, from approximately 08 UT. The second arc "b" forms some time before 09 UT adjacent to the dusk sector oval, before moving from dusk to dawn during period II after the transition in B_Y. It is also seen in Figure 2f as an enhancement in emission crossing the noon-midnight meridian slightly after 10:00 UT.

Figure 3 presents a sequence of images showing the evolution of the arcs "a" and "b." This figure includes images from both IMAGE/WIC and DMSP/SSUSI. The IMAGE/WIC data show dayglow in the saturated dayside areas of each relevant panel. In IMAGE/WIC data from the Southern Hemisphere, TPA "a" appears first at approximately 08:06 UT, toward the dawnside (panel iii). TPA "b" appears slightly later, in the duskside flank at approximately 08:59 UT (panel x). Arc "a" is almost stationary and becomes almost indeterminable from the area of dawnside auroral oval emission, whereas arc "b" moves across the polar cap from the dusk to the dawnside, eventually colliding with the original arc "a" (panel xvii). SSUSI images, taken using the Lyman-Birge-Hopfield short (LBHs) filter (140 to 150 nm), are shown in panels vi–vii, xiii–xiv, xx–xxi, and xxvii–xxviii. We plot SSUSI images for each hemisphere for each polar pass between 07:00 UT and 13:00 UT. The UT for each SSUSI panel indicates the midtime of the polar region pass. Comparing all passes of the Southern Hemisphere (vii, xiv, xxi, and xxviii), SSUSI sees the same auroral features (TPAs "a" and "b") observed by IMAGE (although limited by the extent of the swaths). All passes of the Northern Hemisphere during the period when the TPAs are observed by IMAGE (xiii, xx, xxvii) show the same auroral features, but reflected in position about the noon-midnight meridian. The commencement of the substorm as shown by the growth of

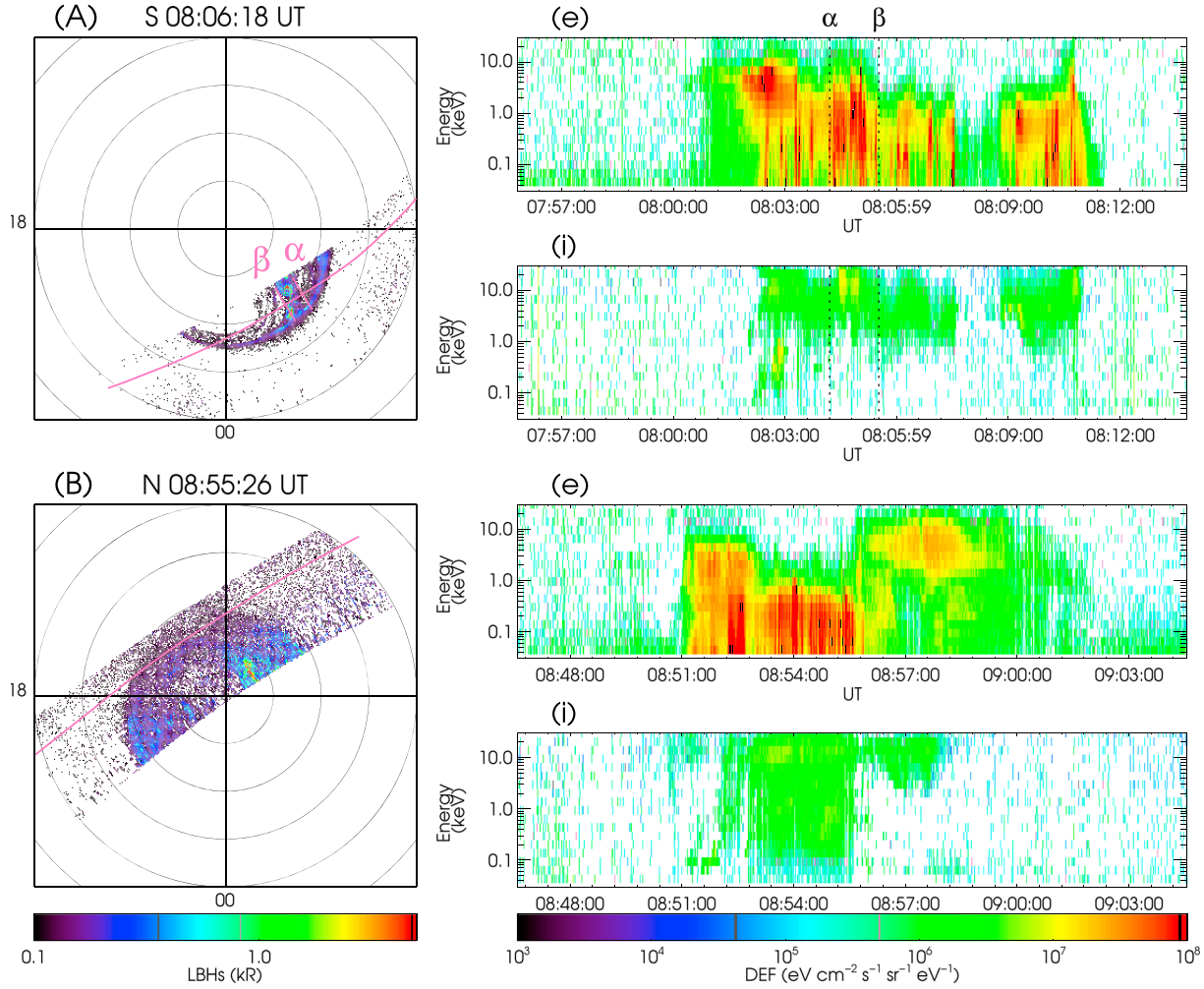

Figure 5. DMSP satellite tracks and spectrograms. The satellite tracks (magenta) are shown across the SSUSI image for the high-latitude pass in the left-hand panels as labeled with a capital letter. Spectrograms are shown in the right-hand panels for electrons "(e)" and ions "(i)". Periods of interest are denoted by Greek letters and dotted lines.

the nightside auroral bulge and the reduction in size of the aurora-free polar cap region, as discussed above with respect to the incoming solar wind conditions, is evident from panel xxiv onward.

In Figure 4 for each row in the first two left-hand columns, we plot a Northern Hemisphere SSUSI image, accompanied by the SuperDARN ionospheric flow velocities along with the calculated electrostatic equipotential patterns (calculated using the technique of *Ruohoniemi and Baker* [1998]) at a time when the DMSP satellite had crossed halfway across the polar cap (see the label above the panels). We repeat these two panels in the right-hand columns of each row, with cartoon positions of the arcs superimposed on each image, to aid in our discussion. As the SSUSI images shown are for the Northern Hemisphere, TPA "b" is seen to move from dawn to dusk across the polar cap in this sequence. In Figure 4a the convection pattern flow vectors are consistent with the strongly northward IMF observed at this time, that is, reverse (lobe) convection cells. The center of the dawn cell is colocated with the top of arc "b." In Figure 4b, fast antisunward flows are crossing the dayside polar cap boundary, and the electrostatic pattern is representative of ongoing low-latitude dayside reconnection which is consistent with the B_Y-dominated (but slightly northward) IMF conditions at the time. In Figure 4c, a highly asymmetric equipotential pattern is observed, that is also representative of ongoing low-latitude dayside reconnection under B_Y dominant conditions.

In Figure 5 we plot a series of electron and ion spectrograms as measured by the DMSP SSJ4 instrument during its crossing of the polar cap. Each spectrogram pair is accompanied with a panel showing the satellite track (magenta line) across the corresponding SSUSI image for each polar cap pass. Each row is labeled with a capital

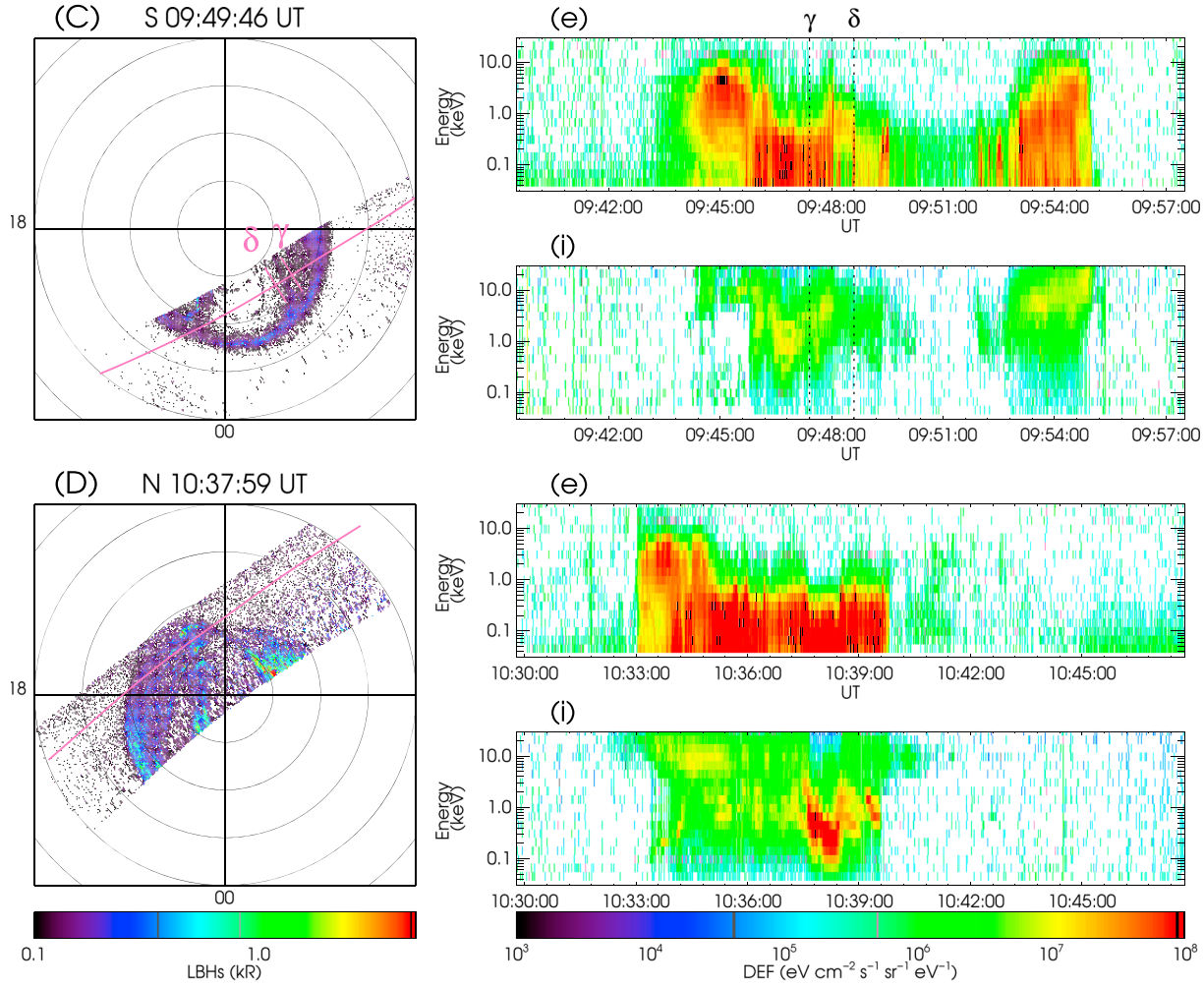

Figure 5. (continued)

letter, placed above the image showing the satellite track, and each spectrogram is either labeled "(e)" for electrons or "(i)" for ions. Times of interest are marked by Greek letters in each plot. Note that the field of view of the SSUSI camera is angled slightly antisunward from the spacecraft. The spectrometers are in situ zenith-directed detectors that are restricted to capture precipitating particles in a narrow field of view, and so only TPAs that are traversed by the satellite track will be detected by the SSJ4 instrument.

In Figure 5A the DMSP satellite, moving from right to left in the image of the Southern Hemisphere pass, crosses over the arc marked "a" in Figure 3, after its ingress into the polar cap region. Within the spectrograms, the crossing of the auroral oval boundary appears as an increase in approximately few keV electrons (Figure 5A.e) up to ~08:03 UT, followed by a drop in energy of the precipitating electrons. Between α and β we see an increase in flux of ~1 keV electrons, followed by a reduction of detected particles, excluding the short excursions to higher fluxes that appear associated with later small-scale structure that is at the limit of detectability in Figure 5A. The period between α and β corresponds to the traversal of the TPA-associated emission, as marked by the cross-track bars in the SSUSI image of Figure 5A. As the satellite exits the polar cap region an increase in fluxes and energies of electrons is noted, at around ~08:10 UT. The ion data of Figure 5A.i are less clear, although a slight increase in flux is seen between α and β.

Figures 5B and 5D show that during these Northern Hemisphere passes, the DMSP satellite only skimmed the dayside portion of the polar cap region, without traversing any enhanced emission regions we associate with a TPA.

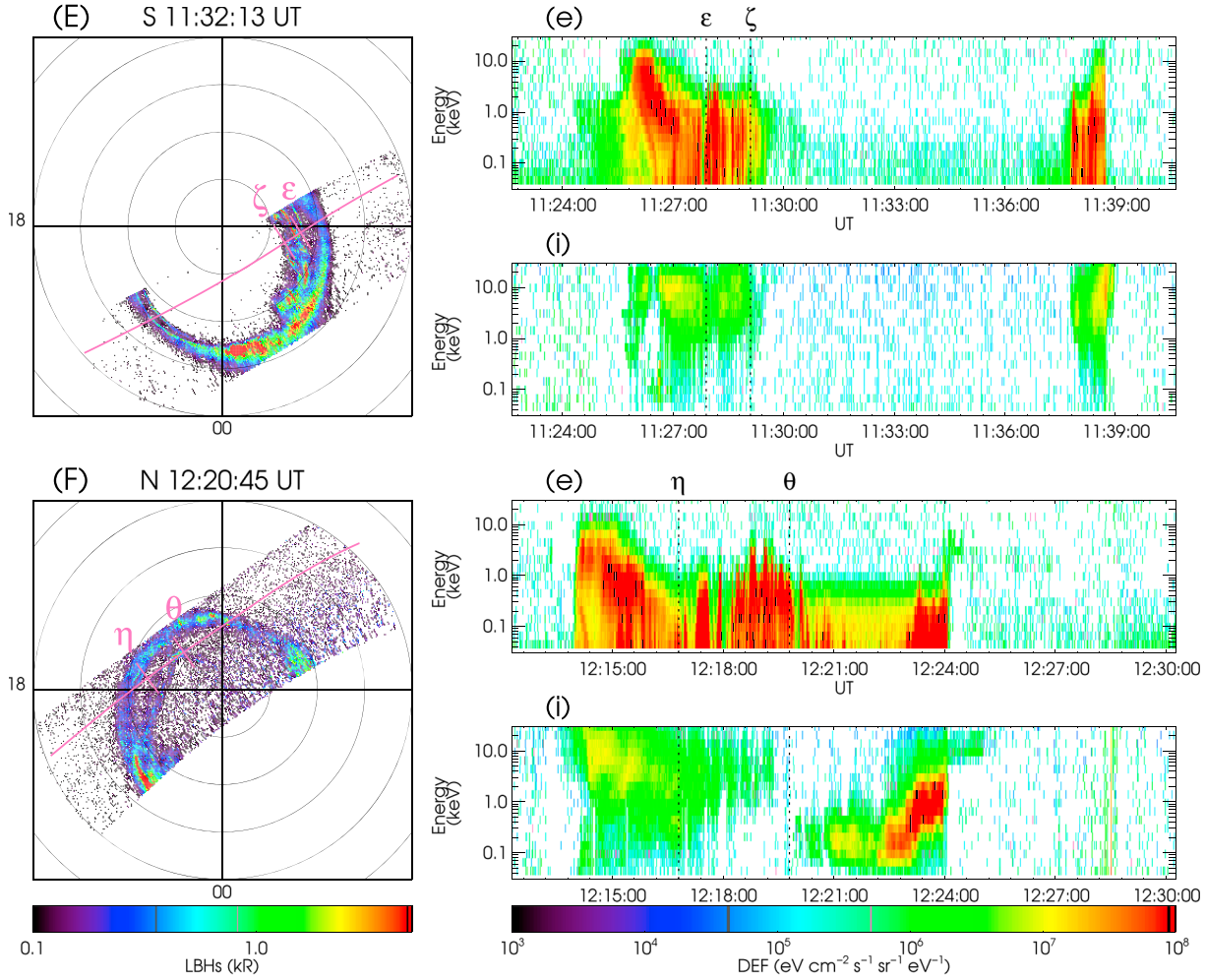

Figure 5. (continued)

Figure 5C and spectrograms (Figure 5C.e and Figure 5C.i) exhibit similar signatures to those of Figure 5A, whereby there is an increase in energy in both the electron and ion spectrograms, as marked between γ and δ. The traversal of TPA "a" is delimited by γ and δ in both the images from SSUSI and the spectrograms. Again, the auroral oval boundary crossing is visible in the electron data, as in Figure 5A.e. A less dramatic drop in energies is seen at these boundary crosses in the ion data.

Figure 5D as mentioned previously is much like Figure 5B. The ion fluxes at approximately 10:37 UT, however, showed a marked increase, which we associate with the traversal of the cusp spot (more commonly associated with proton aurora, under northward IMF conditions, and here associated with IMF B_y-dominated conditions [e.g., *Fear et al.*, 2015; *Milan et al.*, 2000]).

Figure 5E shows the next Southern Hemisphere pass. A short gap between the auroral oval crossing and a period of enhanced electron fluxes is shown immediately prior to ϵ, which lasts until ζ (Figure 5E.e). The ion fluxes also increased between ϵ and ζ (Figure 5E.i). The period between ϵ and ζ covers the traversal of the increased emission, marked by the cross-track bars in the SSUSI image, which we associate with the TPA, as previously observed in Figures 5A and 5C. After this period the satellite passes into the open polar cap region when little particle precipitation is detected.

Figure 5F shows the only Northern Hemisphere pass when the satellite clips the enhanced emission region of a TPA. The auroral oval boundary crossing is noted in all panels (Figures 5F, 5F.e, and 5F.i) prior to ~12:16 UT. There follows a period of intermittent enhanced electron precipitation at high fluxes but at lower energies to the boundary crossing (Figure 5F.e), as marked between η and θ in both the SSUSI image and spectrograms. These signatures are less clear in the proton data of Figure 5F.i. As the satellite leaves the polar cap at around

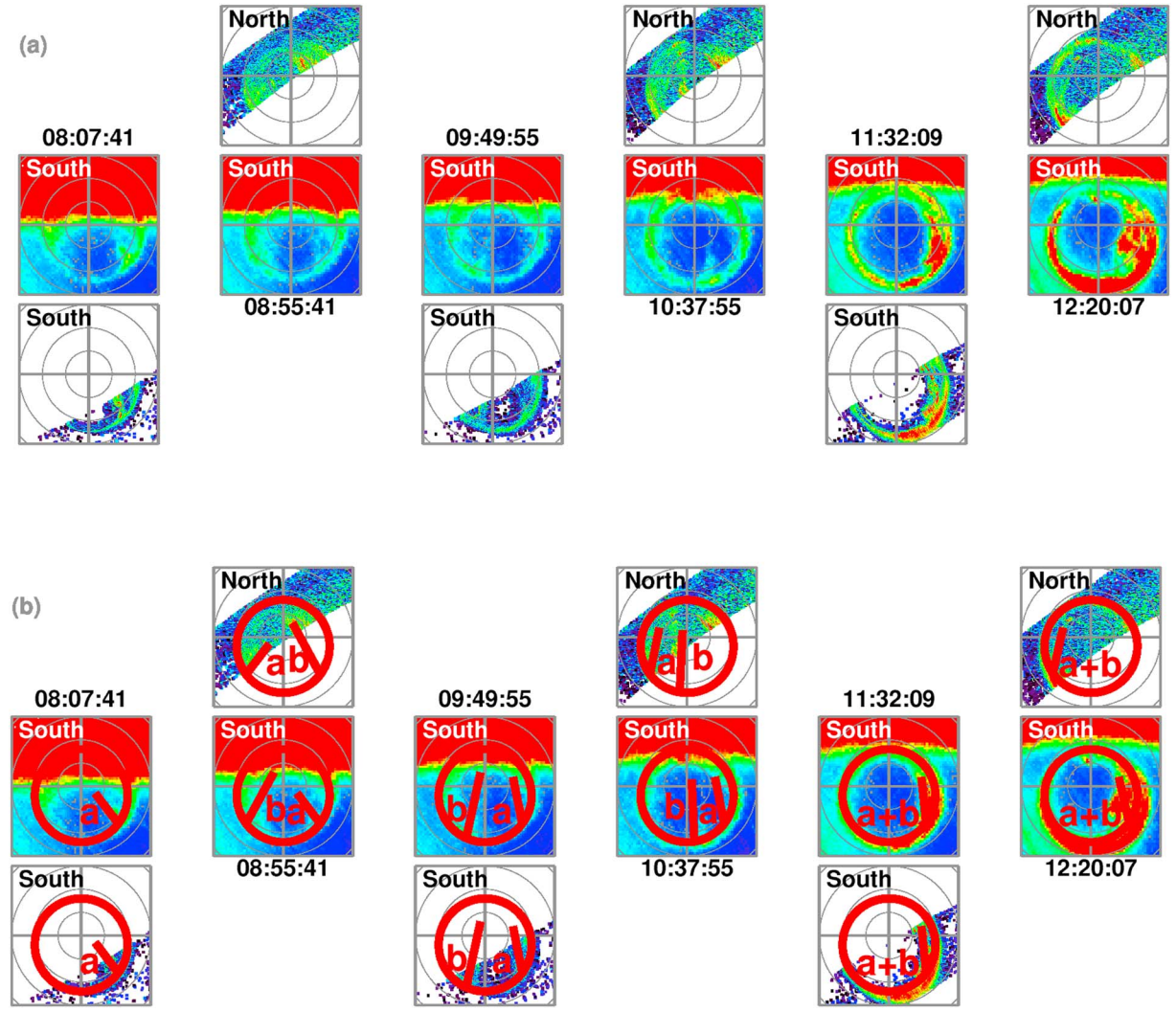

Figure 6. (a) A selected sequence of SSUSI (for the Northern/Southern Hemispheres for the top/bottom rows, respectively) and IMAGE/WIC (middle row, Southern Hemisphere only) images. The times relevant to each panel are given above or below each column of images. (b) The sequence is repeated as in Figure 6a, with cartoon positions of the TPAs superimposed on each image. Noon/dawn is toward the top/right of each panel.

noon, a dispersed ion signature is seen in the precipitating protons (Figure 5F.i), and an increase in fluxes is seen in the electrons (Figure 5F.e).

3. Discussion

We have presented auroral observations of two TPAs present in both the Northern and Southern Hemispheres on 31 August 2005, along with supporting data of the ambient solar wind and geomagnetic conditions, and the ionospheric convection at the time of the observations. One of the arcs, "a," is almost static and stays close to the main auroral oval, whereas the other, "b," was seen to move across almost the entire polar cap.

To aid in the visualization of the movement of the arcs, we refer to Figure 6. In this figure we present a select set of IMAGE/WIC and SSUSI images from the time series for our day of interest (Figure 6a). We repeat the same sequence of images in the figure, along with superimposed cartoons of the arcs in each panel (Figure 6b).

The emission around the Northern Hemisphere arc "a" (SSUSI image, Figure 6, at ~08:55 UT) is diffuse and spatially broad. However, the presence of emission at this location, in the otherwise dark region of the polar cap, is consistent with the position of the TPA in the mirror position about midnight but in the Southern Hemisphere (at approximately 09:49 UT in Figure 6). In addition, the position of the arc detected in the Southern Hemisphere SSUSI images is consistent with the position of the same arc observed by IMAGE/WIC

(see the panels at 08:07 UT of Figure 6). Therefore, given the positions of the arc at first appearance, the observations are consistent with the model of *Milan et al.* [2005] whereby the footprint of TPA arc "a" will be seen at mirror positions about the midnight meridian in each hemisphere (Figure 1). The location of formation of the arc is determined by the upstream IMF B_Y component sometime prior to the arc's formation. Following solar wind propagation tailward, the IMF B_Y component is introduced into the tail with some delay [*Browett et al.*, 2017]. In the *Milan et al.* [2005] model, the amount of twisting in the tail (applied to the layer immediately above the magnetotail current sheet) due to the IMF B_Y component at the time of a period of tail reconnection will determine the MLT location of the TPA at its formation. Via the *Milan et al.* [2005] model, the position of arc "a" at formation implies that the IMF B_Y component was positive some hours prior to the arcs' appearance. While there is evidence that the IMF B_Y component controls the location of arc formation [e.g., *Fear and Milan*, 2012a], there is still some uncertainty about the simplicity of this relationship. The position of the "a" arc is fairly static throughout the arc's lifetime. The lack of movement of arc "a" indicates that the convection pattern in the polar cap at this instance prevents the arc from much movement. The movement of arc "a" is discussed further in terms of the Northern Hemisphere convection patterns, as measured by SuperDARN, later in this section. In the Southern Hemisphere arc "a" may be restricted in motion by the small-sized dawn cell under initially northward IMF, with negative B_Y, and non-B_Y dominated conditions. However, we are limited in considering convection pattern data from the Northern Hemisphere only, so few conclusions about movement in the Southern Hemisphere can be drawn.

A thin bright area of emission appears in the DMSP/SSUSI Northern Hemisphere data at 08:55 UT of Figure 6. We associate this emission with the noon tip of arc "b" as labeled in the IMAGE/WIC image at 09:18 UT of Figure 3ix. The "b" arc seen by the SSUSI cameras during the southern pass (Figure 6 at 09:49 UT) is consistent with the nightside location of the arc as obtained by IMAGE/WIC. The starting positions of "b" in each hemisphere (which from Figure 2g appears to form sometime between 08:00 and 09:00 UT) are mirrored about the midnight meridian, consistent with the *Milan et al.* [2005] model. Due to the differing positions of arc "b" and arc "a" at formation, the IMF B_Y component that had been introduced into the tail at the time of formation of arc "a" was in the opposite sense to that of arc "b." During period I, when both arcs form, the polar cap contracts slightly in size as explained by the Expanding Contracting Polar Cap (ECPC) model [*Cowley and Lockwood*, 1992; *Milan et al.*, 2012, and references therein]. A contraction is associated with net nightside reconnection (and subsequent redistribution of closed flux around the polar cap), which is a feature also consistent with the *Milan et al.* [2005] model of TPA evolution. We postulate that most of the closed flux that results from the nightside reconnection results in the appearance of the TPAs, rather than purely large-scale contractions of the polar cap.

The "b" arc is seen to move steadily across the entire polar cap during period II in response to the change in the upstream B_Y component, crossing midnight at approximately 10:06 UT, as previously noted in the keograms of Figures 2f and 2g, and as shown at 10:37 UT of Figure 6. The orientation of the upstream IMF B_Y component will determine the contemporary convection pattern within the polar cap. The "b" arc moves across the polar cap in opposite directions in each hemisphere, so that the "b" arc moves toward dusk in the Northern Hemisphere and dawn in the Southern Hemisphere. The *Milan et al.* [2005] model (their Figure 9b) predicts that a TPA may move across the whole polar cap (from dawn to dusk for the Northern Hemisphere), for the case where IMF $B_Y > 0$ and $B_Y| > B_Z$, given a single lobe cell with clockwise convection. For the case where IMF $B_Y > 0$ but $|B_Y| < B_Z$, the expected Northern Hemisphere ionospheric convection pattern would contain two cells consisting of a large dawn and a small dusk cell [*Milan et al.*, 2005, Figure 9a]. In this scenario, the duskward movement of an arc would be limited to the duskward extreme of the dawn cell. Throughout the majority of the arcs' lifetimes, the IMF B_Y component is positive and strongly dominates that of the IMF B_Z component, so it may be anticipated that an arc would move across the entire polar cap.

Under such dominant B_Y conditions, it is possible for low-latitude dayside reconnection to take place, even though the B_Z component is positive (northward). As such, open flux is expected to be added to the dayside polar cap, increasing the size of the polar cap region so that the main auroral oval expands to lower latitudes (as explained by the ECPC model), as observed during period II. Due to the large IMF B_Y component, the addition of open flux will be asymmetric about the noon meridian, being added to the dawnside of the dayside polar cap in the Northern Hemisphere,or the duskside in the Southern Hemisphere. Once arc "b" has moved across the polar cap toward the dawnside (Southern Hemisphere), the arcs are no longer distinguishable (Figure 6 at 11:32 UT and 12:20 UT). This is seen in Figures 2f and 2g. The final suppression of the arcs is preceded by a brightening of the dawnside auroral oval (period III) and the commencement of a substorm

following a southward turning of the IMF (period IV). In Figure 2f and 2g we observe the steady expansion of the polar cap region, as determined from the equatorward motion of the auroral oval boundary to lower latitudes. The polar cap then begins to contract following the commencement of the substorm, as noted in both the brightening of the auroral oval nightside bulge and the auroral indices in Figure 2e.

In Figure 4 we consider ionospheric flows observed in the Northern Hemisphere. In Figure 4a we plot the SSUSI Northern Hemisphere image when the arcs were first observed. The IMF dial in the top right of the panel indicates that at this point the IMF was not B_Y dominated and was northward. The multicell equipotential convection patterns shown overlaid on the SSUSI image at this point are consistent with northward IMF conditions, with lobe stirring occurring about noon. The dawn reverse cell occurs near the tip of TPA "b," as indicated in the mechanism of the motion of a TPA as described in *Milan et al.* [2005]. In Figure 4b, at the approximate midpoint of the arcs' evolution, strong antisunward flow is seen, as indicated by the fast and strongly azimuthal flows seen across the dayside polar cap boundary. The asymmetric two-cell equipotential patterns and flows are indicative of dayside reconnection, albeit under slightly northward and IMF B_Y-dominated conditions, as indicated by the IMF dial. This is consistent with the expansion of the polar cap seen during period II. IMF B_Y is strongly positive at this point and the fast flows (red) indicate that additional open flux is being added to the polar cap regions in the dawn sector. The addition of open flux under IMF B_Y positive conditions will cause an asymmetric redistribution of newly open flux to the polar cap, and as such the dawn cell and dusk cells will be in themselves asymmetric. In the *Milan et al.* [2005] model, the TPA, on closed field lines, is entrained in the flow of the surrounding open flux of the polar cap. Under IMF B_Y-dominated conditions, the addition of flux in the larger dawn cell to the dawnside of the TPA causes the duskward motion of the TPA. Both arcs "a" and "b" move to the duskside (Northern Hemisphere). Arc "a" originates far on the (northern) duskside and moves only slightly duskward to eventually lie beside the boundary of the auroral oval where it can no longer move. Arc "b," however, shows the largest movement almost across the entire polar cap. This situation is similar to that observed by *Goudarzi et al.* [2008] and is consistent with the *Milan et al.* [2005] model of TPA formation and subsequent motion. Fast flows are also seen in Figure 4c, and at this point the IMF has turned slightly southward, although IMF B_Y at this time still dominates. This panel illustrates the conditions of ionospheric convection just before the arcs are finally suppressed following a southward turning of the IMF and the commencement of a substorm.

Spectrograms and satellite passes across the polar cap are shown in Figure 5. The DMSP satellite passed very close to the main auroral oval, meaning that any particle precipitation signatures are difficult to isolate. Even so, increased electron fluxes are seen when the arcs are traversed, with more subtle signatures in the ion data. Previous studies of transpolar arcs have been able to separate bursts of increased electron and ion fluxes at energies of a few hundreds of eV, embedded within a clear period of homogeneous polar rain [*Newell and Meng*, 1995; *Newell et al.*, 1997]. These bursts were identified as particle precipitation from plasma sheet fragments, and the energies observed are similar to those of the enhancements identified at the points of the TPA crossings, as presented in this paper. *Watanabe and Hairston* [2016] identified crossings of a set of TPAs in several DMSP passes of both the Northern and Southern Hemispheres. In these cases, DMSP traversed the TPAs close to the midnight meridian which allowed for a greater separation of the signatures of the auroral oval and TPA precipitation. However, the energies of both electrons and ions selected as associated with TPAs by *Watanabe and Hairston* [2016] are analogous to those identified in this paper.

The *Milan et al.* [2005] model of TPA formation suggests that an arc is linked between hemispheres on common closed field lines otherwise embedded in a region of open field lines in the remainder of the polar cap. These field lines traverse the midnight meridian at some point down the tail. Comparisons between TPA formation models, specifically those that rely on the influence of the IMF B_Y component, have been presented in *Fear and Milan* [2012a] (their Table 1). The data presented here are consistent with a closed field line topology and therefore eliminate those models requiring TPAs to form on open field lines [*Chiu et al.*, 1985; *Lyons*, 1985; *Sojka et al.*, 1994]. The data here also eliminate (as did *Fear and Milan* [2012a]) those models that require a sudden change in IMF orientation to provoke the (near-immediate) formation of an arc, as no such change was seen [*Newell and Meng*, 1995; *Chang et al.*, 1998; *Kullen*, 2000]. Furthermore, the motion of TPA "b" across the polar cap following an IMF B_Y sign change (which followed the initial appearance of the arc), allows us to exclude models which do not incorporate a mechanism for TPA motion [*Makita et al.*, 1991]. For completeness, although better tested using the statistical results of *Fear and Milan* [2012a], the remaining models discussed by *Fear and Milan* [2012a] are excluded as the arcs do not appear following a substorm [*Rezhenov and Vardavas*, 1995], and there is no indication of a B_X dependence [*Reiff and Burch*, 1985]. Arc "a" formed prior to arc "b,"

and therefore under the *Milan et al.* [2005] model, its closed field lines will lie closer to Earth than those that connect arc "b" between the hemispheres. The arcs also form on opposite sides of the nightside polar cap and at conjugate positions between the hemispheres. In addition arc "b" is observed to move from one side of the polar cap to the other. A complex magnetic field line topology, resulting in the coexistence of two tongues of closed field lines protruding into the otherwise open polar cap, is implied by the formation and evolution of these arcs. This implies that there will be two equatorial-crossing field lines (compared to the example single line as shown in Figure 1). The first of these field lines, which is associated with the first arc to form, must cross the equator nearer the Earth than the second, which in turn is associated with the formation of the second arc at some later time.

4. Conclusions

We have presented data from two different spacecraft with imaging instrumentation that have simultaneously observed two TPAs in both Northern and Southern Hemispheres. The observations are consistent with the hypothesis that, under the *Milan et al.* [2005] model of TPA formation, TPAs will initially form at mirror positions about the midnight meridian in opposite hemispheres. In this model, subsequent movement and evolution of the arcs after formation can be independent between the hemispheres and is determined by the particular ionospheric convection patterns in each hemisphere. The *Milan et al.* [2005] model requires a closed-field topology, so the observations present here provide supporting evidence for closed field line models for TPA formation, following the conclusions of statistical and individual TPA studies [*Fear and Milan*, 2012a; *Fear et al.*, 2014]. However, these conclusions remain somewhat controversial within the community, and the data presented here provide a somewhat rare opportunity for an in-depth study using simultaneous observations from a range of spacecraft and ground-based sources to detect and monitor a set of TPAs.

The two TPAs were observed during a time period of about 4 h using the DMSP (F16) and IMAGE spacecraft. Data from the DMSP/SSUSI instrument is sparse, due to the frequency of the high-latitude passes and the restricted field of view, as compared to images of the entire polar region that were obtained with the WIC instrument on board the high-altitude spacecraft IMAGE. However, images from DMSP/SSUSI have allowed us to track the evolution of the two arcs in both hemispheres. We observed that the initial positions of the arcs are consistent with mirror positions about the midnight meridian. The motion of the arcs is consistent with SuperDARN measurements of Northern Hemisphere ionospheric convection, under strongly IMF B_Y dominated but northward conditions. The starting positions of the arcs are consistent with the *Milan et al.* [2005] model of TPA formation, whereby a closed field line region can build up at a MLT sector that represents the twist in the tail introduced by the (upstream) IMF B_Y component, sometime before the arcs' appearance. In addition, although we are limited in observations of the ionospheric convection patterns to only one hemisphere, the evolution of the arcs in the Northern Hemisphere is also expected under the model. Particle precipitation data suggest that the arcs are formed by incoming trapped plasma sheet electrons, via a tongue of closed field protruding into the otherwise open polar cap. The result presented supports the hypothesis that TPAs are formed on closed field lines and are entrained within the ambient ionospheric convection. The arcs are finally suppressed following a southward turning of the IMF that precedes a substorm involving intense brightenings and widenings of the emission associated with the main auroral oval. After the commencement of the substorm, both arcs are no longer visible, being indistinguishable from the main auroral oval.

The formation and evolution of two TPAs, that first appear on opposite sides of the polar cap in one hemisphere and at conjugate positions about midnight in the other hemisphere, suggests an interesting and complex magnetic topology.

Acknowledgments

J.A.C. and S.E.M. gratefully acknowledge support from the STFC consolidated grants ST/K001000/1 and ST/N000749/1. The work at the Birkeland Centre for Space Science is supported by the Research Council of Norway under contract 223252/F50. R.C.F. is supported by STFC Ernest Rutherford FellowshipST/K004298/2. M.-T.W. was supported by a studentship from the Science and Technology Facilities Council, UK. B.H. is supported by the Belgian Fund for Scientific Research. Solar wind data were obtained from the NASA/GSFC OMNI facility (http://omniweb.gsfc.nasa.gov). The DMSP/SSUSI data were obtained from http://ssusi.jhuapl.edu). We are grateful to the principal investigator of the DMSP SSJ4 instrument for the provision of precipitating ion data (http://cindispace.utdallas.edu/DMSP/dmsp_data_at_utdallas.html). IMAGE data were obtained from http://image.gsfc.nasa.gov. SuperDARN data can be obtained via the Virginia Tech facility (http://vt.superdarn.org).

References

Berkey, F. T., L. L. Cogger, S. Ismail, and Y. Kamide (1976), Evidence for a correlation between Sun-aligned arcs and the interplanetary magnetic field direction, *Geophys. Res. Lett.*, *3*, 145–147, doi:10.1029/GL003i003p00145.

Browett, S. D., R. C. Fear, A. Grocott, and S. E. Milan (2017), Timescales for the penetration of IMF B_y into the Earth's magnetotail, *J. Geophys. Res. Space Physics*, *122*, 579–593, doi:10.1002/2016JA023198.

Carter, J. A., S. E. Milan, R. C. Fear, A. Kullen, and M. R. Hairston (2015), Dayside reconnection under interplanetary magnetic field B_y-dominated conditions: The formation and movement of bending arcs, *J. Geophys. Res. Space Physics*, *120*, 2967–2978, doi:10.1002/2014JA020809.

Chang, S.-W., et al. (1998), A comparison of a model for the theta aurora with observations from Polar, Wind, and SuperDARN, *J. Geophys. Res.*, *103*, 17,367–17,390, doi:10.1029/97JA02255.

Chisham, G., et al. (2007), A decade of the Super Dual Auroral Radar Network (SuperDARN): Scientific achievements, new techniques and future directions, *Surv. Geophys.*, *28*, 33–109, doi:10.1007/s10712-007-9017-8.

Chiu, Y. T., N. U. Crooker, and D. J. Gorney (1985), Model of oval and polar cap arc configurations, *J. Geophys. Res.*, *90*, 5153–5157, doi:10.1029/JA090iA06p05153.
Cowley, S. W. H., and M. Lockwood (1992), Excitation and decay of solar wind-driven flows in the magnetosphere-ionosphere system, *Ann. Geophys.*, *10*, 103–115.
Craven, J. D., J. S. Murphree, L. L. Cogger, and L. A. Frank (1991), Simultaneous optical observations of transpolar arcs in the two polar caps, *Geophys. Res. Lett.*, *18*, 2297–2300, doi:10.1029/91GL02308.
Fear, R. C., and S. E. Milan (2012a), The IMF dependence of the local time of transpolar arcs: Implications for formation mechanism, *J. Geophys. Res.*, *117*, A03213, doi:10.1029/2011JA017209.
Fear, R. C., and S. E. Milan (2012b), Ionospheric flows relating to transpolar arc formation, *J. Geophys. Res.*, *117*, A09230, doi:10.1029/2012JA017830.
Fear, R. C., S. E. Milan, R. Maggiolo, A. N. Fazakerley, I. Dandouras, and S. B. Mende (2014), Direct observation of closed magnetic flux trapped in the high latitude magnetosphere, *Science*, *346*, 1506–1510, doi:10.1126/science.1257377.
Fear, R. C., S. E. Milan, J. A. Carter, and R. Maggiolo (2015), The interaction between transpolar arcs and cusp spots, *Geophys. Res. Lett.*, *42*, 9685–9693, doi:10.1002/2015GL066194.
Frank, L. A., J. D. Craven, J. L. Burch, and J. D. Winningham (1982), Polar views of the Earth's aurora with Dynamics Explorer, *Geophys. Res. Lett.*, *9*, 1001–1004, doi:10.1029/GL009i009p01001.
Goudarzi, A., M. Lester, S. E. Milan, and H. U. Frey (2008), Multi-instrumentation observations of a transpolar arc in the Northern Hemisphere, *Ann. Geophys.*, *26*, 201–210, doi:10.5194/angeo-26-201-2008.
Grocott, A., S. W. H. Cowley, and J. B. Sigwarth (2003), Ionospheric flow during extended intervals of northward but B_y-dominated IMF, *Ann. Geophys.*, *21*, 509–538, doi:10.5194/angeo-21-509-2003.
Grocott, A., S. Badman, S. Cowley, T. Yeoman, and P. Cripps (2004), The influence of IMF B_y on the nature of the nightside high-latitude ionospheric flow during intervals of positive IMF B_z, *Ann. Geophys.*, *22*, 1755–1764, doi:10.5194/angeo-22-1755-2004.
Gusev, M. G., and O. A. Troshichev (1986), Hook-shaped arcs in dayside polar cap and their relation of the IMF, *Planet. Space Sci.*, *34*, 489–496, doi:10.1016/0032-0633(86)90087-5.
Gussenhoven, M. S. (1982), Extremely high latitude auroras, *J. Geophys. Res.*, *87*, 2401–2412, doi:10.1029/JA087iA04p02401.
Huang, C. Y., J. D. Craven, and L. A. Frank (1989), Simultaneous observations of a theta aurora and associated magnetotail plasmas, *J. Geophys. Res.*, *94*(A8), 10,137–10,143, doi:10.1029/JA094iA08p10137.
Hubert, B., J.-C. Gérard, S. Fuselier, S. Mende, and J. Burch (2004), Proton precipitation during transpolar auroral events: Observations with the IMAGE-FUV imagers, *J. Geophys. Res.*, *109*, A06204, doi:10.1029/2003JA010136.
King, J. H., and N. E. Papitashvili (2005), Solar wind spatial scales in and comparisons of hourly Wind and ACE plasma and magnetic field data, *J. Geophys. Res.*, *110*, A02104, doi:10.1029/2004JA010649.
Kullen, A. (2000), The connection between transpolar arcs and magnetotail rotation, *Geophys. Res. Lett.*, *27*(1), 73–76, doi:10.1029/1999GL010675.
Kullen, A., M. Brittnacher, J. A. Cumnock, and L. G. Blomberg (2002), Solar wind dependence of the occurrence and motion of polar auroral arcs: A statistical study, *J. Geophys. Res.*, *107*, 1362, doi:10.1029/2002JA009245.
Lyons, L. R. (1985), A simple model for polar cap convection patterns and generation of auroras, *J. Geophys. Res.*, *90*(A2), 1561–1567, doi:10.1029/JA090iA02p01561.
Makita, K., C.-I. Meng, and S.-I. Akasofu (1991), Transpolar auroras, their particle precipitation, and IMF by component, *J. Geophys. Res.*, *96*(A8), 14,085–14,095, doi:10.1029/90JA02323.
Mende, S. B., et al. (2000a), Far ultraviolet imaging from the IMAGE spacecraft. 2. Wideband FUV imaging, *Space Sci. Rev.*, *91*, 271–285.
Mende, S. B., et al. (2000b), Far ultraviolet imaging from the IMAGE spacecraft. 1. System design, *Space Sci. Rev.*, *91*, 243–270.
Milan, S. E., M. Lester, S. W. H. Cowley, and M. Brittnacher (2000), Dayside convection and auroral morphology during an interval of northward interplanetary magnetic field, *Ann. Geophys.*, *18*(4), 436–444, doi:10.1007/s00585-000-0436-9.
Milan, S. E., B. Hubert, and A. Grocott (2005), Formation and motion of a transpolar arc in response to dayside and nightside reconnection, *J. Geophys. Res.*, *110*, A01212, doi:10.1029/2004JA010835.
Milan, S. E., J. S. Gosling, and B. Hubert (2012), Relationship between interplanetary parameters and the magnetopause reconnection rate quantified from observations of the expanding polar cap, *J. Geophys. Res.*, *117*, A03226, doi:10.1029/2011JA017082.
Newell, P. T., and C.-I. Meng (1995), Creation of theta-auroras: The isolation of plasma sheet fragments in the polar cap, *Science*, *270*, 1338–1341, doi:10.1126/science.270.5240.1338.
Newell, P. T., D. Xu, C.-I. Meng, and M. G. Kivelson (1997), Dynamical polar cap: A unifying approach, *J. Geophys. Res.*, *102*(A1), 127–139, doi:10.1029/96JA03045.
Obara, T., M. Kitayama, T. Mukai, N. Kaya, J. S. Murphree, and L. L. Cogger (1988), Simultaneous observations of Sun-aligned polar cap arcs in both hemispheres by Exos-C and Viking, *Geophys. Res. Lett.*, *15*(7), 713–716, doi:10.1029/GL015i007p00713.
Østgaard, N., S. B. Mende, H. U. Frey, L. A. Frank, and J. B. Sigwarth (2003), Observations of non-conjugate theta aurora, *Geophys. Res. Lett.*, *30*, 2125, doi:10.1029/2003GL017914.
Paxton, L. J., D. Morrison, Y. Zhang, H. Kil, B. Wolven, B. S. Ogorzalek, D. C. Humm, and C.-I. Meng (2002), Validation of remote sensing products produced by the Special Sensor Ultraviolet Scanning Imager (SSUSI): A far UV-imaging spectrograph on DMSP F-16, in *Proceedings of Optical Spectroscopic Techniques, Remote Sensing, and Instrumentation for Atmospheric and Space Research IV*, vol. 4485, edited by A. M. Larar and M. G. Mlynczak, pp. 338–348, Society of Photo-Optical Instrumentation Engineers (SPIE) Conference Series, SPIE, San Diego, Calif., doi:10.1117/12.454268.
Reidy, J. A., R. C. Fear, D. K. Whiter, B. Lanchester, A. J. Kavanagh, L. J. Paxton, Y. Zhang, and M. Lester (2017), Multi-instrument observation of simultaneous polar cap auroras on open and closed magnetic field lines, *J. Geophys. Res.*, *122*, 4367–4386, doi:10.1002/2016JA023718.
Reiff, P. H., and J. L. Burch (1985), IMF B(y)-dependent plasma flow and Birkeland currents in the dayside magnetosphere. II—A global model for northward and southward IMF, *J. Geophys. Res.*, *90*, 1595–1609, doi:10.1029/JA090iA02p01595.
Rezhenov, B. V., and I. M. Vardavas (1995), A possible mechanism for <theta> aurora formation, *Ann. Geophys.*, *13*, 698–703, doi:10.1007/s00585-995-0698-3.
Ruohoniemi, J. M., and K. B. Baker (1998), Large-scale imaging of high-latitude convection with Super Dual Auroral Radar Network HF radar observations, *J. Geophys. Res.*, *103*, 20,797–20,811, doi:10.1029/98JA01288.
Sojka, J. J., L. Zhu, D. J. Crain, and R. W. Schunk (1994), Effect of high-latitude ionospheric convection on Sun-aligned polar caps, *J. Geophys. Res.*, *99*(A5), 8851–8863, doi:10.1029/93JA02667.
Watanabe, M., and M. R. Hairston (2016), Observation of a unipolar field-aligned current system associated with IMF B_y-triggered theta auroras, *J. Geophys. Res. Space Physics*, *121*, 4483–4497, doi:10.1002/2015JA022016.